Equilibrium dynamics of the sub-Ohmic spin-boson model under bias*

Da-Chuan Zheng(郑大川) and Ning-Hua Tong(同宁华)†

Department of Physics, Renmin University of China, Beijing 100872, *China*

(Received 21 January 2017; revised manuscript received 23 February 2017; published online 20 April 2017)

Using the bosonic numerical renormalization group method, we studied the equilibrium dynamical correlation function $C(\omega)$ of the spin operator σ_z for the biased sub-Ohmic spin-boson model. The small-ω behavior $C(\omega) \propto \omega^s$ is found to be universal and independent of the bias ε and the coupling strength α (except at the quantum critical point $\alpha = \alpha_c$ and $\varepsilon = 0$). Our NRG data also show $C(\omega) \propto \chi^2\omega^s$ for a wide range of parameters, including the biased strong coupling regime ($\varepsilon \neq 0$ and $\alpha > \alpha_c$), supporting the general validity of the Shiba relation. Close to the quantum critical point α_c, the dependence of $C(\omega)$ on α and ε is understood in terms of the competition between ε and the crossover energy scale ω_0^* of the unbiased case. $C(\omega)$ is stable with respect to ε for $\varepsilon \ll \varepsilon^*$. For $\varepsilon \gg \varepsilon^*$, it is suppressed by ε in the low frequency regime. We establish that $\varepsilon^* \propto (\omega_0^*)^{1/\theta}$ holds for all sub-Ohmic regime $0 \leqslant s < 1$, with $\theta = 2/(3s)$ for $0 < s \leqslant 1/2$ and $\theta = 2/(1+s)$ for $1/2 < s < 1$. The variation of $C(\omega)$ with α and ε is summarized into a crossover phase diagram on the α–ε plane.

Keywords: spin-boson model, numerical renormalization group, quantum phase transition, dynamical correlation function

PACS: 05.10.Cc, 05.30.Jp, 64.70.Tg, 75.20.Hr **DOI:** 10.1088/1674-1056/26/6/060501

1. Introduction

The spin-boson model (SBM) is one of the simplest models to describe a quantum two-level system coupled to the environmental noise.[1,2] It has realizations in various fields of physics, including the superconducting qubit,[3] mesoscopic metal ring penetrated by an Aharonov–Bohm flux,[4] ultraslow glass dynamics,[5] heavy fermion metals,[6] and nanomechanical oscillators,[7] etc. In this model, the environmental noise is represented by a bath of harmonic oscillators with the low frequency spectral function characterized by $J(\omega) \propto \alpha\omega^s$. Here α is the coupling constant and s is a dimensionless parameter that discriminates the Ohmic ($s = 1$), super-Ohmic ($s > 1$), and sub-Ohmic ($0 \leqslant s < 1$) bath.

The SBM has been studied in detail for the Ohmic and weak-coupling regime to understand the quantum decoherence and dissipation, which are the key issues for making a long-lived quantum bit,[3] chemical reaction,[8] as well as in the optical absorption in a quantum dot.[9] The SBM without a bias field also contains non-trivial quantum phase transitions (QPTs) between a weak-coupling delocalized phase and a strong-coupling localized phase for $0 \leqslant s \leqslant 1$. It is an established result that a Kosterlitz–Thouless-type QPT exists for $s = 1$ and the ground state is always delocalized for $s > 1$.[1,2] In the sub-Ohmic regime $0 \leqslant s < 1$,[1,2,10] numerical methods such as numerical renormalization group (NRG),[11–13] quantum Monte Carlo (QMC),[14] and exact diagonalization[15] show that a continuous QPT occurs at certain critical coupling α_c, at which both the static and the dynamic quantities show critical behavior.[16–25]

For the study of both decoherence and QPT, the equilibrium dynamical correlation function is an important quantity. Most of the previous studies concentrate on the case of zero bias and weak coupling, *i.e.*, $\varepsilon = 0$ and $\alpha < \alpha_c$. In this regime, the $\sigma_z - \sigma_z$ correlation function $C(\omega)$ (to be defined below) shows a power law behaviour $C(\omega) \sim \omega^s$ in small frequency $\omega \ll \omega_0^*$ and critical behavior $C(\omega) \sim \omega^{-s}$ in the intermediate frequency $\omega_0^* \ll \omega \ll \omega_0$. Here ω_0 is a non-universal high energy scale and ω_0^* is the crossover energy scale between the delocalized fixed point and the quantum critical fixed point.

The situation with a finite bias $\varepsilon \neq 0$, however, has received less attention. For $\varepsilon \neq 0$, the parity symmetry of the unbiased SBM is broken and hence the localized–delocalized QPT of the sub-Ohmic symmetric SBM no longer exists. Instead, as the coupling strength increases, the ground state changes smoothly from the biased weak-coupling delocalized-like state to the strong-coupling localized-like state with broken symmetry. The strong coupling regime is difficult to describe for the perturbation-based theory.[18] For numerical approaches such as NRG[11,12] and exact diagonalaization,[15] a finite bias increases the number of bosons in the ground state and makes an accurate calculation more difficult. As a result, systematic study of the dynamical correlation function for the

*Project supported by the National Basic Research Program of China (Grant No. 2012CB921704), the National Natural Science Foundation of China (Grant No. 11374362), the Fundamental Research Funds for the Central Universities, China, and the Research Funds of Renmin University of China (Grant No. 15XNLQ03).

†Corresponding author. E-mail: nhtong@ruc.edu.cn

© 2017 Chinese Physical Society and IOP Publishing Ltd

sub-Ohmic bath under a finite bias, especially in the strong coupling regime $\alpha > \alpha_c$, is still lacking.

In this paper, we use NRG to study the equilibrium state dynamical correlation function of the sub-Ohmic SBM with a finite bias field $\varepsilon \neq 0$, with emphasis on the strong-coupling regime $\alpha > \alpha_c$. By carefully extrapolating the boson-state truncation to infinity, we find that except for the exact QPT point, $C(\omega)$ always obeys $\chi^2\omega^s$ behavior in the small frequency limit, irrespective of the values of ε and α. In the vicinity of the quantum critical point (QCP), $C(\omega)$ is characterized by two different power law regimes: $C(\omega) \propto \omega^s$ in the low frequency regime $\omega \ll \omega^*$ and $C(\omega) \propto \omega^{-s}$ in the intermediate frequency regime $\omega^* \ll \omega \ll \omega_0$, with ω_0 being a non-universal high energy scale. The crossover frequency ω^* is tuned by ε. For weak bias $\varepsilon \ll \varepsilon^*$, $\omega^* = \omega_0^* \propto |\alpha - \alpha_c|^{z\nu}$ and $C(\omega)$ is not changed significantly from the zero bias case. For strong bias $\varepsilon \gg \varepsilon^*$, $\omega^* \propto \varepsilon^\theta$ and $C(\omega)$ is suppressed in $\omega \ll \omega^*$. The behavior of ω^* is understood in terms of the competition between the unbiased crossover scale ω_0^* and ε, and we have $\omega^* \sim max\left[\varepsilon^\theta, \omega_0^*\right]$. We obtained the critical exponent θ as a function of s. The crossover bias ε^* is thus determined as $\varepsilon^* = (\omega_0^*)^{1/\theta}$. We finally summarize the behavior of $C(\omega)$ in a crossover $\varepsilon - \alpha$ phase diagram.

This paper is organized as the following. In Section 2 we introduce SBM and the formalism we used to calculate the equilibrium correlation function with thev bosonic NRG method. Section 3 presents the results from our NRG study. A conclusion is given in Section 4.

2. Model and method

The Hamiltonian of SBM reads

$$H = -\frac{\Delta}{2}\sigma_x + \frac{\varepsilon}{2}\sigma_z + \sum_i \omega_i a_i^\dagger a_i + \frac{\sigma_z}{2}\sum_i \lambda_i (a_i + a_i^\dagger). \quad (1)$$

The first two terms describe a two level system with bias ε and tunnelling strength Δ. The bosonic bath is described by the third term, where ω_i is the frequency of the i-th boson mode. In the last term, the two level system is coupled to the bosonic bath through σ_z and the boson displacement operator. Various experimental realizations of this Hamiltonian have been proposed with tunable parameters ε and Δ.[4,26–28] The influence of the bath on the two level system is characterized by the spectral function

$$J(\omega) = \pi \sum_i \lambda_i^2 \delta(\omega - \omega_i). \quad (2)$$

In this paper, we use a power law form of $J(\omega)$ with a hard cut-off at ω_c,

$$J(\omega) = 2\pi\alpha\omega^s\omega_c^{1-s}, \quad (0 \leqslant \omega \leqslant \omega_c). \quad (3)$$

We set $\omega_c = 1.0$ as the unit of energy and fix $\Delta = 0.1$ to study the dependence of equilibrium dynamics on ε and α for a sub-Ohmic bath.

At $\varepsilon = 0$, equation (1) is invariant under the combined boson and spin parity transformation $Ua_iU^{-1} = -a_i$ and $U\sigma_zU^{-1} = -\sigma_z$. For the sub-Ohmic ($0 \leqslant s < 1$) and the Ohmic ($s = 1$) baths, a spontaneous breaking of this symmetry may occur in the regime $\alpha > \alpha_c$ and the system enters the localized phase, in which the quantum system is trapped to one of the two states and the local bosons have a finite displacement.[10–15] This is the delocalize–localize quantum phase transition of SBM. With a finite bias $\varepsilon \neq 0$, the above parity symmetry is broken from the outset and the phase transition no longer exists. As α increases, the ground state crosses over smoothly from the weak-coupling to the strong-coupling biased states.

In this paper, we focus on the $\sigma_z - \sigma_z$ dynamical correlation function defined as

$$C(\omega) = \frac{1}{2\pi}\int_{-\infty}^{+\infty} C(t)\,\mathrm{e}^{\mathrm{i}\omega t}\,\mathrm{d}t, \quad (4)$$

where $C(t) = (1/2)\langle[\sigma_z(t), \sigma_z(0)]_+\rangle$ and $[\hat{A}, \hat{B}]_+$ is the anti-commutator of $\hat{A}$ and $\hat{B}$. For a non-degenerate ground state, the Lehman representation of the correlation function at $T = 0$ is written as

$$\begin{aligned} C(\omega) = {} & \frac{1}{2}\sum_n |\langle 0|\sigma_z|n\rangle|^2 \delta(\omega + E_0 - E_n) \\ & + \frac{1}{2}\sum_n |\langle n|\sigma_z|0\rangle|^2 \delta(\omega + E_n - E_0). \end{aligned} \quad (5)$$

Here $|n\rangle$ and E_n are the n-th eigen state and energy of the Hamiltonian, respectively. $C(\omega)$ has the general form $C(\omega) = A\delta(\omega) + C'(\omega)$, where $A = |\langle 0|\sigma_z|0\rangle|^2$ and $|0\rangle$ is the ground state. It is an even function of ω and fulfils the sum rule

$$\int_{-\infty}^{+\infty} C(\omega)\,\mathrm{d}\omega = 1. \quad (6)$$

The bosonic NRG method is regarded as one of the most accurate numerical techniques for studying SBM due to its non-perturbative nature and the applicability in the whole range of parameters.[11,12,29,30] The success of NRG relies on the energy scale separation due to the logarithmic discretization, and on the RG transformation which is carried out by iterative diagonalization in each energy shell. It is technically composed of three steps: logarithmic discretization, transforming the Hamiltonian into a semi-infinite chain, and the iterative diagonalization. In general, the errors in the NRG calculation come from two sources. One is the approximation of using one bath mode to represent each energy shell, which is controlled by the logarithmic discretization parameter $\Lambda \geqslant 1$. The other is the truncation of the energy spectrum after each diagonalization to overcome the exponential increase of the

Hilbert space, which is controlled by the number of kept states M_s. For the bosonic NRG, an additional source of error is the truncation of infinite dimensional Hilbert space of each boson mode into N_b states on the occupation basis. Exact results are obtained in the limit $\Lambda = 1$, $M_s = \infty$, and $N_b = \infty$.

In practice, however, one cannot do the calculation directly at the above limit and extrapolating NRG data to the above limit could be difficult. In the strong coupling regime with a bias, the ground state has a large boson number and hence requires a large N_b for an accurate calculation. A large N_b, however, will increase the truncation error because in the NRG calculation only the lowest $1/N_b$ fraction of the eigen states of the previous energy shell are kept for constructing the Hamiltonian of the lower energy shell. To keep the accuracy, one has to use a larger Λ to increase the energy separation of successive energy shells. This in turn will lead to a larger discretization error of the bath. Fortunately, we found that a larger Λ only induces quantitative changes to the NRG results and the qualitative conclusion can still be obtained reliably. Therefore, using a large $\Lambda = 2 \sim 10$, a moderate $M_s \sim 100 \sim 200$, and $N_b = 12 \sim 60$, we can obtain qualitatively correct results for the biased SBM in the strong coupling regime. Combining the knowledge gained from the finite size scaling method of N_b,[31,32] we checked that our final conclusions are stable when extrapolated to the exact limit. To calculate $C(\omega)$, we use the patching method of Bulla[33] with which the sum rule Eq. (6) is fulfilled reasonably well. The discrete δ peaks obtained are broadened with a Gaussian function on the logarithmic scale,[33]

$$\delta(\omega-\omega_n) \to \frac{\mathrm{e}^{-b^2/4}}{b\omega_n\sqrt{\pi}} \exp\left[-\frac{(\ln\omega - \ln\omega_n)^2}{b^2}\right]. \tag{7}$$

We choose the broadening parameter $b = 0.7$ for $\Lambda < 4$ and $b = 1.2$ for $\Lambda \geqslant 4$.

3. Results

In this work, we study the dynamical correlation function $C(\omega)$ for all the range of α and $\varepsilon \neq 0$. As ε tends to zero, the strong coupling phase of $\alpha > \alpha_c$ is continuously connected to the localized state at $\varepsilon = 0$ with spontaneously broken symmetry. At $\varepsilon = 0$ and $\alpha > \alpha_c$, the localized state without symmetry breaking is special in that the ground state has a two-fold degeneracy and it is unstable in the thermodynamical limit.[34] In this paper we hence confine our study to the symmetry-broken phase (either spontaneously or by a finite bias) and do not study that special case.

3.1. ω^s-behavior in the small frequency regime

For the Ohmic ($s = 1$) and the super-Ohmic ($s > 1$) baths, the small frequency behavior of $C(\omega)$ in the delocalized phase obeys the Shiba relation,[35] which in our notation reads[12]

$$C(w) = \frac{\alpha}{4}\chi^2\omega^s, \quad (\omega \to 0). \tag{8}$$

Here $\chi \equiv 2\partial\langle\sigma_z\rangle/\partial\varepsilon|_{\varepsilon=0}$ is the local spin susceptibility. The proof in Ref. [35] applies also to the case with a finite bias, but not to the localized phase at $\alpha > \alpha_c$ for the Ohmic bath. This exact relation was used to test the quality of various approximate results for SBM.[11,12,19,36–39]

There have been attempts to generalize the Shiba relation to (i) sub-Ohmic bath, (ii) with finite bias, and (iii) strong coupling regime $\alpha > \alpha_c$. Such a generalized relation, if it exists, would imply a universal long time behavior $C(t) \propto t^{-(1+s)}$ for any s values, coupling strength α (except at the critical point $\alpha = \alpha_c$ and $\varepsilon = 0$), and spin parameters Δ and ε. Up to now these activities received partial success only. Florens and others[40] proved Eq. (8) for the sub-Ohmic bath, based on an exact relation from the perturbation theory in Majorana representation. However, their proof applies only to delocalized phase at the symmetry point $\varepsilon = 0$. The numerical results from the approximate perturbation theory built on a unitary transformation fulfils Eq. (8) exactly for the sub-Ohmic bath with[41,42] or without[18] bias in the weak to intermediate coupling. In the strong coupling regime $\alpha > \alpha_c$ the fulfilment is good but not exact. This leaves the question open whether the Shiba relation holds in the biased strong coupling regime of the sub-Ohmic SBM.

As stated above, the inherent truncation errors of NRG hinder it from the quantitative confirmation/falsification of the generalized Shiba relation. However, qualitatively, it is possible to check the factors on the right-hand side of Eq. (8) each for a time. In this section, we will show that $C(\omega) \propto \omega^s$ holds for the sub-Ohmic SBM with general α and ε. In Fig. 6, data are presented to further support that $C(\omega)/\omega^s \propto \chi^2$ for general α and ε values.

In Fig. 1, we first present the N_b-dependence of $C(\omega)$ obtained from NRG under bias, in order to gauge the choice of N_b in our study. The energy flows (Fig. 1(a)) and $C(\omega)$ (Fig. 1(b)) are shown for a sub-Ohmic bath $s = 0.8$ in the strong coupling regime $\alpha = 0.5 > \alpha_c$, with a finite bias $\varepsilon = 10^{-3}$. We use a series of N_b values from $N_b = 8$ to $N_b = 40$ with $\Lambda = 4$ and $M_s = 120$. In Fig. 1(a), for a given N_b, the excitation energies $\Lambda^N[E_i(N) - E_0(N)]$ ($i = 1,2,3$) first flow to an unstable fixed point (with $\Lambda^N[E_1(N) - E_0(N)] \approx 0.61$) in the small N regime. After a crossover N^*, they flow to the stable fixed point (with $\Lambda^N[E_1(N) - E_0(N)] \approx 0.77$) in the large N limit. We found that the unstable fixed point in the small N regime is the same as the weak-coupling fixed point of the SBM in the non-bias case (dashed lines obtained using $\alpha = 0$ and $\varepsilon = 0$). With N_b increasing geometrically, the crossover N^* increases linearly, showing that the associated energy scale $T^* \sim \Lambda^{-N^*}$ decreases to zero as a negative power of N_b. This supports that

the unstable fixed point (dashed lines in Fig. 1(a)) will extend to infinitely large N in the limit $N_b = \infty$ and it is the true fixed point of the biased SBM. In this biased fixed point, ε flows to infinity and the spin is effectively decoupled from the bath, leading to the same excitation levels as the free boson chain.

Figure 1(b) shows the corresponding $C(\omega)$, which has two different power-law regimes: $C(\omega) \sim \omega^{y_l}$ in the low frequency regime $\omega \ll \omega^*$, and $C(\omega) \sim \omega^{y_h}$ in the high frequency regime $\omega \gg \omega^*$. NRG data for $s = 0.8$ gives $y_l = 2.07$ and $y_h = 0.799$. With increasing N_b, the crossover frequency ω^* decreases to zero as a negative power of N_b, proving that $C(\omega) \sim \omega^{y_h}$ is the correct result of the biased SBM (dashed line in Fig. 1(b)). Our results for other s values in $1/2 \leqslant s \leq 1$ agree with $y_h = s$ within an error of 2% (not shown).

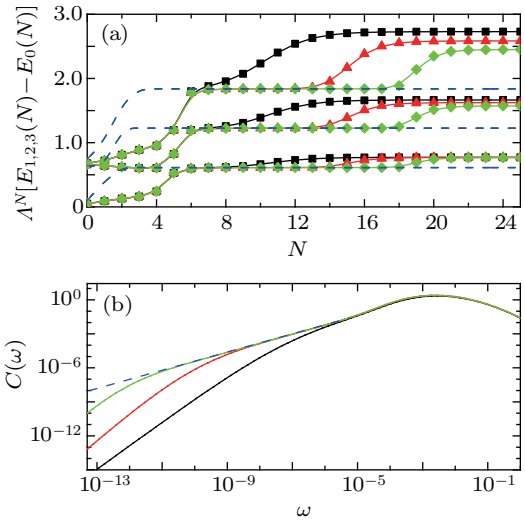


Fig. 1. (color online) NRG flow diagrams and $C(\omega)$ at $s = 0.8$, $\Delta = 0.1$, $\alpha = 0.5 > \alpha_c$, and $\varepsilon = 10^{-3}$. (a) Flow diagrams obtained using $N_b = 8$, 18, and 40 (symbols with eye-guiding lines, from left to right). The dashed lines are the flow of $\alpha = 0$ and $\varepsilon = 0$. (b) Dynamical correlation function $C(\omega)$ for $N_b = 8$, 18, and 40 (solid lines, from bottom to top), and $N_b = \infty$ from extrapolation (dashed lines). Fitting the small ω regime, we obtain the exponents $y_l = 2.07$ for $N_b = 8$, and $y_h = 0.799$ for $N_b = \infty$. The $\delta(\omega)$ peak is not shown. NRG parameters are $\Lambda = 4.0$ and $M_s = 120$.

For $s < 1/2$, the NRG results converge with much more difficulty with increasing N_b. In Fig. 2, we show the strong coupling data ($\alpha = 0.045 > \alpha_c$) for $s = 0.3$. Both the energy flow and $C(\omega)$ have N_b-dependent crossover scales. With N_b increasing to 60, a clear trend can be seen that the N_b-converged levels flow towards the free boson energy levels (Fig. 2(a)). For both $\varepsilon = 10^{-2}$ and $\varepsilon = 10^{-3}$, the section of $C(\omega)$ with ω^s behavior extends to smaller ω with increasing N_b (Fig. 2(b)). The shift of $C(\omega)$ with N_b has an apparent scaling form and an analysis for N_b could be carried out to extract the correct exponent, as done in Ref. [31]. Here in Fig. 2(b), we only mark out the expected asymptotic ω^s line for guiding the eye. With this understanding of the N_b-dependence of $C(\omega)$, in the rest of this paper, we only show the physically correct results $C(\omega > \omega^*)$ obtained using sufficiently large N_b.

In Fig. 3, we investigate the influence of ε on $C(\omega)$ for α values ranging from weak coupling $\alpha < \alpha_c$ (Fig. 3(a)) to strong coupling $\alpha > \alpha_c$ (Fig. 3(b)) for $s = 0.8$ and $\Delta = 0.1$. It is seen that $C(\omega) \sim \omega^s$ in the small frequency limit for all parameters. In Fig. 3(a), for the small coupling $\alpha = 0.1$ (dash-dotted lines), $C(\omega)$ does not change with ε up to $\varepsilon = 10^{-3}$ and the three curves for $\varepsilon = 0$, 10^{-3}, and 10^{-5} overlap. While for a moderate coupling $\alpha = 0.4$ (dashed lines), a slight downward shift is observed between $\varepsilon = 10^{-3}$ and $\varepsilon = 10^{-5}$ and the lines for $\varepsilon = 0$ and 10^{-5} overlap. $C(\omega)$ is most sensitive to ε when α is close to $\alpha_c \approx 0.482$. The same trend is observed in Fig. 3(b) for the strong coupling regime.

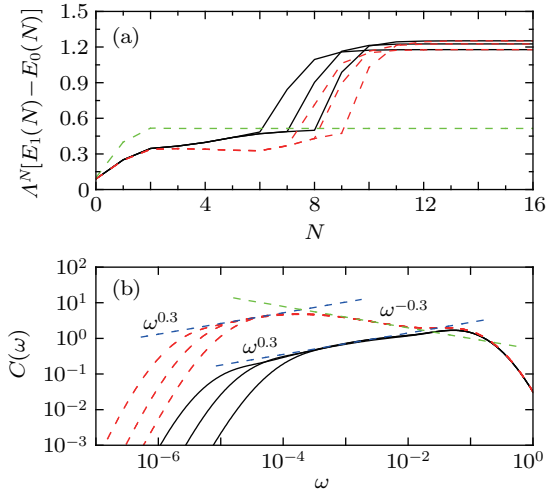


Fig. 2. (color online) NRG flow diagrams and $C(\omega)$ at $s = 0.3$, $\Delta = 0.1$, $\alpha = 0.045 > \alpha_c$. $\varepsilon = 10^{-2}$ (solid lines) and $\varepsilon = 10^{-3}$ (dashed lines). (a) Flow diagrams obtained using $N_b = 12$, 27, and 60 (from left to right). The horizontal dashed lines are the flow of $\alpha = 0$ and $\varepsilon = 0$. (b) $C(\omega)$ for $N_b = 12$, 27, and 60 (from bottom to top). The functions $\omega^{0.3}$ and $\omega^{-0.3}$ are marked by the dashed straight lines for guiding the eye. The $\delta(\omega)$ peak is not shown. NRG parameters are $\Lambda = 4.0$ and $M_s = 120$.

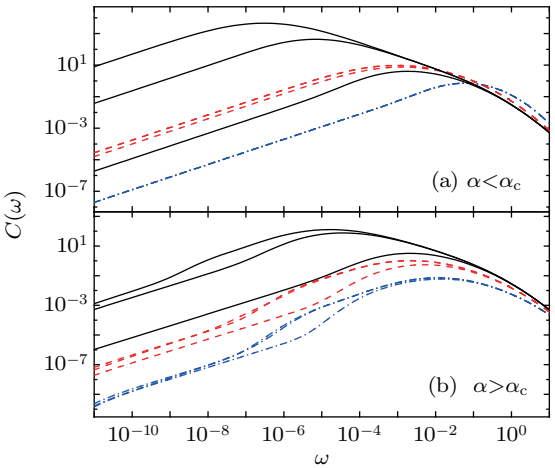


Fig. 3. (color online) $C(\omega)$ for various α and ε at $s = 0.8$, $\Delta = 0.1$. (a) $\alpha < \alpha_c \approx 0.482$: $\alpha = 0.48$ (solid lines), 0.4 (dashed lines), and 0.1 (dash-dotted lines). (b) $\alpha > \alpha_c$: $\alpha = 0.49$ (solid lines), 0.57 (dashed lines), and 0.7 (dash-dotted lines). For each α value, from top to bottom are curves for $\varepsilon = 0$, 10^{-5}, and 10^{-3}. All curves show $C(\omega) \propto \omega^s$ behavior in the small ω limit. NRG parameters are $\Lambda = 4$, $M_s = 120$, and $N_b = 60$.

The universal $C(\omega) \propto \omega^s$ behavior observed so far in Figs. 1, 2, and 3 has a natural understanding. When the parity

symmetry is already broken by a finite bias, the ground state of SBM can be tuned continuously on the α–ε plane, going from a delocalized state at $\alpha < \alpha_c$, $\varepsilon = 0^+$, through a half circle in a finite ε region, to the symmetry-spontaneously-broken state at $\alpha > \alpha_c$, $\varepsilon = 0^+$, without passing the critical point. Therefore, the ground state has the same nature and no qualitative change is expected in the small ω limit of $C(\omega)$. Indeed, our NRG results for different s, α, and ε confirm that $C(\omega) \propto \omega^s$ is a universal feature of SBM.

In the strong coupling case shown in Fig. 3(b), the same tendency is observed, i.e., with increasing ε, $C(\omega)$ shifts downwards and the most prominent change occurs near α_c. The suppression of $C(\omega)$ can be understood as the weight transfer: with increasing ε, $|\langle\sigma_z\rangle|$ increases and so does the weight of the zero-frequency δ peak. Due to the sum rule, $C(\omega > 0)$ decreases uniformly. Comparing Figs. 3(a) and 3(b), one sees that a broad peak forms for $\alpha > \alpha_c$ and $\varepsilon \sim 10^{-3}$.

Besides the universal low frequency behavior of $C(\omega)$ that we focus on in this paper, the high frequency structure in $C(\omega)$ for the deep sub-Ohmic SBM ($s \leqslant 1/2$) has also attracted a great deal of attention recently.[17,18,41] For small s values, a peak at the renormalized tunnelling $\omega = \Delta_r$ is observed in the strong coupling regime. It persists even in the localized phase $\alpha > \alpha_c$. For α close to α_c and small ε, another pronounced peak is observed at the crossover scale $\omega = \omega_0^*$. $C(\omega)$ thus has a two-peak structure for small s and close to the critical point. Here, our $C(\omega)$ for $s = 0.3$ and a weak bias $\varepsilon = 10^{-3}$ does have the two-peak structure, as shown by the dashed lines in Fig. 2(b). The high frequency peak is weak due to the over broadening of the log-Gaussian function. Decreasing the broadening parameter b from 1.2 to 0.8, the high frequency peak gets sharper and more pronounced, being consistent with previous results.[17,18,40]

3.2. Equilibrium dynamics near QCP

In the above section, we established the universal ω^s-behaviour of $C(\omega)$ in the full parameter space of SBM. In this section, we focus on the parameter regime near the QCP $\alpha \sim \alpha_c$ and study the critical properties of $C(\omega)$ under a bias. For the unbiased SBM, $T_0^* \propto |\alpha - \alpha_c|^{z\nu}$ is the only energy scale that controls the crossover between the stable fixed points (localized and delocalized fixed points) and the critical fixed point. Here ν is the critical exponent of the correlation length and $z = 1$ is the dynamical critical exponent. T_0^* plays an important role in the temperature dependence of physical quantities close to QCP. At zero temperature, it also appears in the dynamical correlation function in the delocalized phase: $C(\omega) \sim \omega^s$ for $\omega \ll \omega_0^*$ and $C(\omega) \sim \omega^{-s}$ for $\omega \gg \omega_0^*$, and $\omega_0^* = T_0^*$. $C(\omega) \propto \omega^{-s}$ is the critical behavior which holds for arbitrarily small frequency at the exact critical point $\alpha = \alpha_c$, and is confined to $\omega \gg \omega_0^*$ away from the critical point. As α approaches α_c, ω_0^* tends to zero and the ω^{-s} behavior will be recovered in the full frequency range.

For the biased case, $\varepsilon > 0$ is another energy scale that influences the crossover between different behaviors of $C(\omega)$. Our NRG results for $C(\omega)$ at different α and ε can be understood in terms of the competition between ε and T_0^*. Due to the difficulty of N_b convergence for $0 \leqslant s < 1/2$, here we show NRG data for $s = 0.8$, representing a typical case for $1/2 < s < 1$. Our conclusion also applies to $0 \leqslant s < 1/2$, as will be discussed below.

In Fig. 4 and Fig. 5, we show the flow diagrams (Fig. 4) and $C(\omega)$ (Fig. 5) for $\alpha = 0.3868 < \alpha_c$ (a), $\alpha = 0.4008 > \alpha_c$ (b), and $\alpha = 0.393647 \approx \alpha_c$ (c), respectively. For each α, ε varies from zero to 10^{-3}. The purpose is to observe the influence of ε in the delocalized, localzied, and critical phases. Figures 4(a) and 5(a) are for $\alpha < \alpha_c$. At $\varepsilon = 0$, the energy flow in Fig. 4(a) has a crossover at around $N_0^* \approx 16$ (solid circle), from the critical fixed point to the weak-coupling one. As ε increases from zero, the flow does not change for $\varepsilon < 10^{-5}$ and the crossover N^* (empty squares) begins to decreases only for $\varepsilon > 10^{-4}$. The corresponding evolution of $C(\omega)$ is shown in Fig. 5(a). For $\varepsilon < 10^{-5}$, $C(\omega) \propto \omega^{-s}$ for $\omega \gg \omega_0^* = T_0^*$ and $C(\omega) \propto \omega^s$ for $\omega \ll \omega_0^*$. The crossover scale of the symmetric SBM is given by $\omega_0^* = \Lambda^{-N_0^*} \approx 10^{-5}$. With increasing ε, the crossover frequency ω^* increases and $\omega^* > \omega_0^*$ occurs only when $\varepsilon > 10^{-4}$, corresponding to the occurrence of $N^* < N_0^*$ in the flow diagram. A crossover scale ε^* can be defined as such that for $\varepsilon > \varepsilon^*$, ω^* becomes significantly larger than ω_0^*, or equivalently, $N^* < N_0^*$. For $\varepsilon \ll \varepsilon^*$, $C(\omega)$ stays same as the symmetric case ($\varepsilon = 0$) and $\omega^* = T_0^*$. For $\varepsilon \gg \varepsilon^*$, $C(\omega)$ is suppressed in the low frequency regime and $\omega^* > T_0^*$ is set by ε.

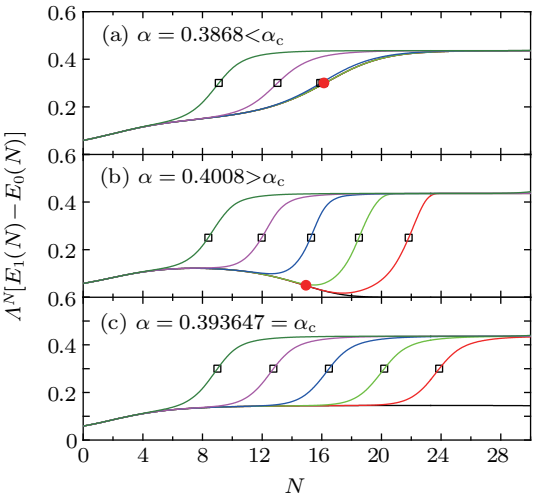


Fig. 4. (color online) (a)–(c) The flow diagrams for three different α values. For each α, from right to left $\varepsilon = 0$, 10^{-7}, 10^{-6}, 10^{-5}, 10^{-4}, and 10^{-3}. The empty squares make out the crossover N^* for the case $\varepsilon > 0$. The solid circle marks out the crossover scale in the unbiased case N_0^*. In panel (c), $N_0^* = \infty$. NRG parameters are $\Lambda = 2.0$, $M_s = 200$, and $N_b = 16$.

Figures 4(b) and 5(b) show the influence of ε in the local-

ized phase. In Fig. 4(b), the excitation energy level at $\varepsilon = 0$ flows from the critical fixed point towards a two-fold degenerate fixed point, with the critical-to-localize crossover around $N^* = N_0^* = 15$ (solid circle). Now we study the change of N^* under bias (empty squares). With a vanishingly small ε, the degeneracy is lifted and the excited energy level has an upturn at an arbitrarily large $N^* \gg N_0^*$, showing a crossover from the localized symmetric state to the biased state. We find that the crossover energy scale $T^* \equiv \Lambda^{-N^*} \propto \varepsilon$. With further increasing ε, the upturn moves to the left and for $\varepsilon > \varepsilon^*$, $N^* < N_0^*$ occurs, which means that N^* is now the crossover from the critical fixed point to the biased fixed point. NRG data give the critical-to-biased crossover $T^* \propto \varepsilon^\theta$. The critical exponent θ will be discussed with Fig. 5(c).

In Fig. 5(b), the evolution of $C(\omega)$ with ε is shown, which looks similar to the case $\alpha < \alpha_c$. That is, $C(\omega)$ does not change much with ε for $\varepsilon \ll \varepsilon^*$ and begins to be suppressed for $\varepsilon \gg \varepsilon^*$. It is noted that for a given $\varepsilon < \varepsilon^*$, the degenerate-to-biased crossover at $N^* > N_0^*$ in the energy flow has no correspondence in $C(\omega)$: the latter has a perfect ω^s behavior at $\omega \sim \omega^* = \Lambda^{-N^*}$. The crossover in the energy flow will only show up in the temperature dependence of $C(\omega)$.

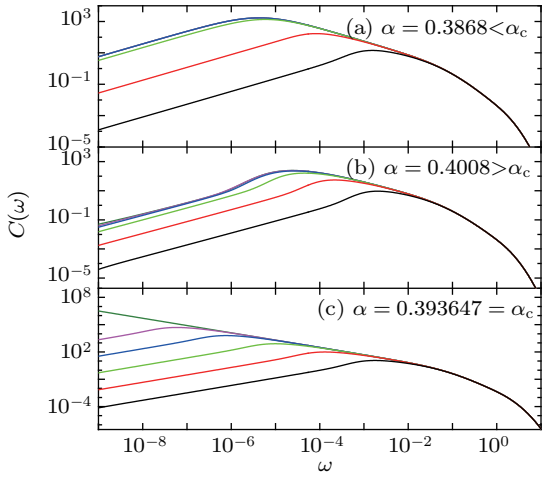


Fig. 5. (color online) (a)–(c): $C(\omega)$ for the same α values. For each α, from top to bottom, $\varepsilon = 0$, 10^{-7}, 10^{-6}, 10^{-5}, 10^{-4}, and 10^{-3}. NRG parameters are the same as Fig. 4.

Figures 4(c) and 5(c) show the influence of ε on the flow and $C(\omega)$ in the critical regime $\alpha \approx \alpha_c$. Since $T_0^* = 0$ at this point, ε is the only energy scale that controls the critical-to-biased crossover in the energy flow and $C(\omega)$. Especially, Fig. 5(c) shows that $C(\omega) \propto \omega^{-s}$ for $\omega \gg \omega^*$ and $C(\omega) \propto \omega^s$ for $\omega \ll \omega^*$. We define a critical exponent θ as

$$\omega^*(\alpha = \alpha_c, \varepsilon) \propto \varepsilon^\theta. \tag{9}$$

For $s = 0.8$, the fitted exponent from Fig. 5(c) is $\theta = 1.12$. Note that the same dependence of ω^* on ε applies to the $\alpha > \alpha_c$ and $\alpha < \alpha_c$ cases in the regime $\varepsilon \gg \varepsilon^*$, which are shown in panels (a) and (b) of Figs. 4 and 5.

The NRG result in Fig. 5(c) shows that for $\alpha = \alpha_c$, $C(\omega \gg \omega^*) \propto c\omega^{-s}$ with an ε-independent factor c. Combining this observation with the assumption that the Shiba relation Eq. (8) holds at $\alpha = \alpha_c$ and $\varepsilon > 0$ (which will be discussed in Fig. 6 below), we can derive θ by equating the small and the large frequency expression at $\omega = \omega^*$, giving

$$(\omega^*)^{-s} \sim \alpha_c [\chi(\alpha_c, \varepsilon)]^2 (\omega^*)^s. \tag{10}$$

Employing the critical behavior $\chi(\alpha_c) \propto \varepsilon^{1/\delta - 1}$, one obtains $\omega^* \propto \varepsilon^{(\delta-1)/(\delta s)}$, giving $\theta = (\delta - 1)/(\delta s)$. From the exact expression $\delta = 3$ for $0 < s < 1/2$ and $\delta = (1+s)/(1-s)$ for $1/2 \leqslant s < 1$, we obtain

$$\theta = \begin{cases} \dfrac{2}{3s}, & \left(0 < s \leqslant \dfrac{1}{2}\right); \\ \dfrac{2}{1+s}, & \left(\dfrac{1}{2} < s < 1\right). \end{cases} \tag{11}$$

For $s = 0.8$, this expression gives $\theta = 1.111$, which agrees well with the NRG result 1.12.

Having shown that $C(\omega) \propto \omega^s$ $(\omega \to 0)$ for general α and ε values in the previous section, we now check the Shiba relation Eq. (8) at $s = 0.8$ using a fixed small frequency $\omega = 1.01561 \times 10^{-8}$. Figure 6 shows $C(\omega)$ and the right-hand side of Eq. (8) $I(\omega) \equiv \alpha\chi^2\omega^s/4$ as functions of ε, for the same α values as in Figs. 4 and 5. We find qualitative agreement between them for a wide range of ε. For $\alpha > \alpha_c$ $(\alpha < \alpha_c)$, $C(\omega)$ shows the crossover from critical (power law dependence on ε) for $\varepsilon \gg \varepsilon^*$ to the localized-like (delocalized-like) behavior (being constant) for $\varepsilon \ll \varepsilon^*$, as expected. For $\alpha = \alpha_c$, a power-law dependence is observed, with the fitted exponent -1.88 (for $C(\omega)$) and -1.84 (for $I(\omega)$), respectively, in reasonable agreement with the exact $2(1/\delta - 1) = -1.78$. It is notable that although $C(\omega)$ and $I(\omega)$ have more than 5 decades of variations in the range $\varepsilon \in [10^{-7}, 10^{-3}]$, their ratio $I(\omega)/C(\omega) = 2 \sim 3$ does not change much. This result supports the relation $C(\omega) \propto \chi^2\omega^s$.

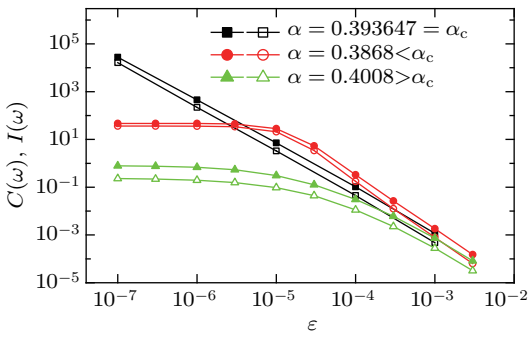


Fig. 6. (color online) Checking the Shiba relation at $s = 0.8$ and $\Delta = 0.1$. $C(\omega)$ (empty symbols) is compared to $I(\omega) \equiv \alpha\chi^2\omega^s/4$ (solid symbols) for various α and ε values. Here $\omega = 1.01561 \times 10^{-8}$. NRG parameters are $\Lambda = 2.0$, $M_s = 200$, and $N_b = 16$.

The ratio also depends weakly on ω due to the slight inaccuracy in the exponent of NRG-produced $C(\omega)$. The uniform

deviation from Eq. (8) observed here is more likely due to the error of NRG data than due to the invalidity of the Shiba relation. After all, a factor of 3 is a reasonable level of error in the NRG calculation of dynamical quantities,[11,12] considering the logarithmic error, truncation errors, as well as the approximation used to calculate $C(\omega)$ and χ.[33] It is expected that the agreement can be improved if we increase M_s and N_b, and extrapolate Λ to unity, which will not be pursued here. The good agreement of the NRG value of the exponent θ and Eq. (11) is also consistent with $C(\omega) \propto \chi^2\omega^s$, since equation (11) is derived from this assumption. For $s = 0.3$, it is more difficult to check the Shiba relation quantitatively due to much stronger boson state truncation error. As shown in Fig. 2(b), using N_b as large as 60, one can obtain the expected ω^s behavior only in a narrow frequency window and for certain ε values. For those parameter regimes and frequencies where ω^s behavior can be obtained, NRG results give a ratio $I(\omega)/C(\omega) = 5 \sim 10$ for the delocalized, critical, and the localized phases, much larger than the $s = 0.8$ case. This shows the difficulty of a quantitatively accurate NRG study for the deep sub-Ohmic SBM.

In Fig. 7(a), we fix $\varepsilon = 10^{-5}$ and plot $C(\omega)$ for different α values. For $\alpha \ll \alpha_c$, $C(\omega)$ increases with increasing α and the height of the peak reaches a maximum at certain $\alpha < \alpha_c$. With further increasing α, $C(\omega)$ begins to decrease uniformly, with the peak height suppressed. In Fig. 7(b), we show the maximum of $C(\omega)$ as functions of α for various ε's. From this figure we can extract the α value at which the height of the peak in $C(\omega)$ reaches the maximum.

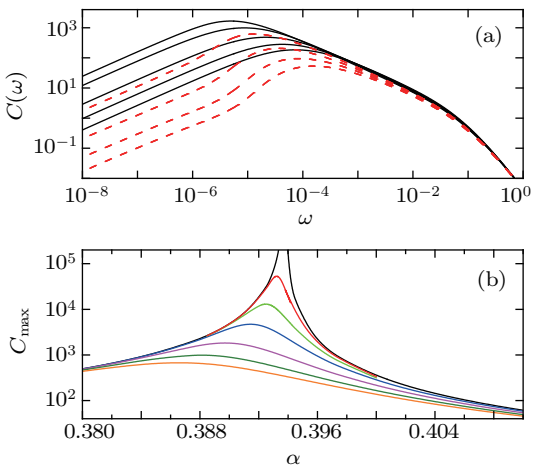


Fig. 7. (color online) (a) $C(\omega)$ at $\varepsilon = 10^{-5}$ and for a series of α's. From top to bottom, $\alpha = 0.39$, 0.385, 0.38, 0.375, and 0.37 (solid lines), and $\alpha = 0.395$, 0.40, 0.405, and 0.41 (dashed lines). (b) The maximum value of $C(\omega)$ as functions of α for a series of ε. From top to bottom, $\varepsilon = 0.0$, 2.0×10^{-7}, 1.0×10^{-6}, 3.0×10^{-5}, 9.0×10^{-6}, 1.8×10^{-5}, and 2.7×10^{-5}. $s = 0.8$, $\Delta = 0.1$. NRG parameters are $\Lambda = 2.0$, $M_s = 100$, and $N_b = 12$.

The phase diagram on the α–ε plane shown in Fig. 8 summarizes our results for $C(\omega)$ near the QCP. Close to α_c and with very small ε, three regions I, II, and III of different nature are separated by a crossover line (squares with eye-guiding line). Regions I and III are continuously connected to the delocalized ($\alpha < \alpha_c$) and localized phase ($\alpha > \alpha_c$) of the symmetric SBM, respectively. They are characterized by $\varepsilon^* \ll T_0^*$. In region I, $\langle\sigma_z\rangle \propto \chi\varepsilon$ with χ being the magnetic susceptibility. In region III, $\langle\sigma_z\rangle \sim -1$ close to the saturate value. For each α, the crossover ε^* in Fig. 8 is defined as the ε value at which the maximum of $C(\omega)$ decreases to 90% of its value at $\varepsilon = 0$.

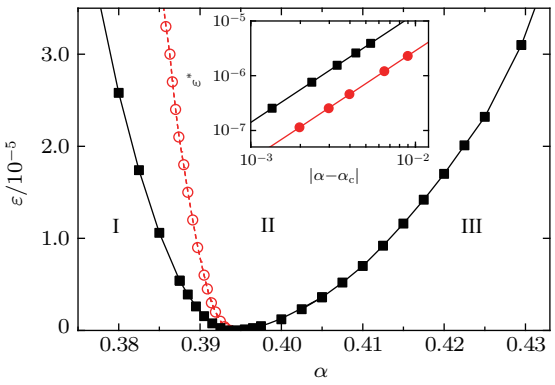


Fig. 8. (color online) Phase diagram of sub-Ohmic SBM near QCP extracted from $C(\omega)$. Regions I, II, and III are the delocalized, quantum critical, and the localized phases, respectively. They are separated by a crossover line (solid squares with eye-guiding line) at which the peak height of $C(\omega)$ drops to 90% of its $\varepsilon = 0$ value. The peak height of $C(\omega)$ reaches maximum at the dashed line with empty circles. Inset: log-log plot of ε^* versus $|\alpha - \alpha_c|$ for $\alpha < \alpha_c$ (solid squares) and $\alpha > \alpha_c$ (solid circles). The fitted exponents are 1.989 and 1.985, respectively.

In region II, T_0^* vanishes near α_c and $\varepsilon \gg T_0^*$ becomes the only characteristic energy scale. In this regime, the magnetization $\langle\sigma_z\rangle$ shows the quantum critical behavior as $\langle\sigma_z\rangle \propto \varepsilon^{1/\delta}$, with δ being a critical exponent. The empty circles with eye-guiding line marks out the parameter at which $C(\omega)$ has a highest peak. Both the crossover line $\varepsilon^*(\alpha)$ and the peak position can be extracted from the data in Fig. 7(b). It is observed that the location of the maximum peak resembles that of the maximum of entanglement entropy.[21] This is not a pure coincident since the crossover peak of $C(\omega)$ reflects a strong fluctuation near the critical point and it is therefore naturally related to the entanglement maximum.

In the inset of Fig. 8, we fit the crossover line close to the QCP in a power law

$$\varepsilon^* \propto c|\alpha - \alpha_c|^\eta, \tag{12}$$

with the obtained critical exponent $\eta = 1.99$ for $s = 0.8$. Note that the asymmetry of ε^* in $\alpha > \alpha_c$ and $\alpha < \alpha_c$ regimes means different pre-factors c. Besides using $C(\omega)$ here, the critical behavior of ε^* can also be determined by the scaling form of $\langle\sigma_z\rangle(\alpha, \varepsilon, \Delta)$ obtained from the N_b scaling analysis of the NRG data.[32] These two approaches give consistent results. For the second approach, the N_b scaling analysis of NRG data gives (see Eqs. (31), (33), (35), (36) in Ref. [32])

$$\langle\sigma_z\rangle(\alpha, \varepsilon, \Delta) = m\left[\left(\frac{\tau}{\Delta^{1-s}}\right)^\beta, \left(\frac{\varepsilon}{\Delta}\right)^{1/\delta}\right]. \tag{13}$$

Here $\tau \equiv \alpha - \alpha_c$ and $m(x,y)$ is a two-variable scaling function. By comparing the magnitude of the two variables in Eq. (13), one obtains $\varepsilon^*(\alpha) \propto |\alpha - \alpha_c|^{\beta\delta}$, giving $\eta = \beta\delta$. Here, β is the critical exponent of the order parameter. It is known that for $0 \leqslant s \leqslant 1/2$, $\beta = 1/2$ and $\delta = 3$. For $1/2 < s < 1$, β is a function of s whose explicit expression is unknown yet, and $\delta = (1+s)/(1-s)$.[13,14,31,43,44] The NRG result $\beta\delta = 1.93$ is in reasonable agreement with the fitted exponent $\eta = 1.99$ in the inset of Fig. 8, showing the consistency of the static and dynamical approaches.

For $0 \leqslant s < 1/2$, NRG calculation is hindered by the slow convergence with N_b and it is difficult to obtain the quantitative data. However, we note that the scaling from Eq. (13) is obtained from the NRG calculation combined with the N_b scaling analysis for the full sub-Ohmic regime $0 \leqslant s < 1$. It is stronger than the scaling ansatz of free energy which applies only to the regime $1/2 < s < 1$.[43,44] The two exponents introduced above, θ and η, are not independent. We have $\varepsilon^* \propto |\alpha - \alpha_c|^{\beta\delta} \sim (T^*)^{\beta\delta/(z\nu)}$. This gives $T^* \propto \varepsilon^{z\nu/(\beta\delta)}$, meaning $\theta = z\nu/\eta$. This is a relation independent of the validity of hyperscaling relation.

4. Conclusion

In summary, we use the bosonic NRG method to study the equilibrium dynamics of the sub-Ohmic SBM under a bias. We found that the small ω behavior $C(\omega) \propto \omega^s$ holds for any bias ε and coupling strength α except exactly at the critical point $\alpha = \alpha_c$, $\varepsilon = 0$, where $C(\omega) \propto \omega^{-s}$. Our results strongly support that $C(\omega) \propto \chi^2\omega^s$ in all parameter regimes, including the biased and strong coupling regime. This is in favour of the validity of the generalized Shiba relation in this regime. Close to the QCP, the competition between the energy scale T_0^* and bias ε determines a crossover scale ε^* which separate the weak-biased regime ($\varepsilon \ll \varepsilon^*$) from a strong-biased regime ($\varepsilon \gg \varepsilon^*$). Near the QCP, $\varepsilon^* \propto |\alpha - \alpha_c|^\eta$ with $\eta = \beta\delta$. These results are summarized in the crossover phase diagram on the α–ε plane.

References

[1] Leggett A J, Chakravarty S, Dorsey A T, Fisher M P A, Garg A and Zwerger W 1987 *Rev. Mod. Phys.* **59** 1

[2] Weiss U 1993 *Quantum Dissipative Systems* (Singapore: World Scientific)

[3] Shnirman A, Makhlin Y and Schon G 2002 *Phys. Scr.* **T102** 147

[4] Tong N H and Vojta M 2006 *Phys. Rev. Lett.* **97** 016802

[5] Rosenberg D, Nalbach P and Osheroff D D 2003 *Phys. Rev. Lett.* **90** 195501

[6] Si Q, Rabello S, Ingersent K and Smith J L 2001 *Nature* **413** 804

[7] Seoanez C, Guinea F and Castro Neto A H 2007 *Europhys. Lett.* **78** 60002

[8] Mühlbacher L and Egger R 2004 *Chem. Phys.* **296** 193

[9] Borri P, Langbein W, Schneider S, Woggon U, Sellin R L, Ouyang D and Bimberg D 2001 *Phys. Rev. Lett.* **87** 157401

[10] Kehrein S and Mielke A 1996 *Phys. Lett. A* **219** 313

[11] Bulla R, Tong N H and Vojta M 2003 *Phys. Rev. Lett.* **91** 170601

[12] Bulla R, Lee H J, Tong N H and Vojta M 2005 *Phys. Rev. B* **71** 045122

[13] Guo C, Weichselbaum A, von Delft J and Vojta M 2012 *Phys. Rev. Lett.* **108** 160401

[14] Winter A, Rieger H, Vojta M and Bulla R 2009 *Phys. Rev. Lett.* **102** 030601

[15] Alvermann A and Fehske H 2009 *Phys. Rev. Lett.* **102** 150601

[16] Chin A and Turlakov M 2006 *Phys. Rev. B* **73** 075311

[17] Anders F B, Bulla R and Vojta M 2007 *Phys. Rev. Lett.* **98** 210402

[18] Lü Z G and Zheng H 2007 *Phys. Rev. B* **75** 054302

[19] Zheng H and Lü Z G 2013 *J. Chem. Phys.* **138** 174117

[20] Florens S, Freyn A, Venturelli D and Narayanan R 2011 *Phys. Rev. B* **84** 155110

[21] Le Hur K, Doucet-Beauprè P and Hofstetter W 2007 *Phys. Rev. Lett.* **99** 126801

[22] Yao Y, Duan L, Lü Z, Wu C Q and Zhao Y 2013 *Phys. Rev. E* **88** 023303

[23] Liu H B, An J H, Chen C, Tong Q J, Luo H G and Oh C H 2013 *Phys. Rev. A* **87** 052139

[24] Kast D and Ankerhold J 2013 *Phys. Rev. Lett.* **110** 010402

[25] Nalbach P and Torwart M 2012 *Phys. Rev. B* **81** 054308

[26] Le Hur K 2012 *Phys. Rev. B* **85** 140506

[27] Goldstein M, Devoret M H, Houzet M and Glazman L I 2013 *Phys. Rev. Lett.* **110** 017002

[28] Egger D J and Wilhelm F K 2013 *Phys. Rev. Lett.* **111** 163601

[29] Bulla R, Costi T A and Pruschke T 2008 *Rev. Mod. Phys.* **80** 395

[30] Wilson K G 1975 *Rev. Mod. Phys.* **47** 773

[31] Hou Y H and Tong T H 2010 *Eur. Phys. J. B* **78** 127

[32] Tong N H and Hou Y H 2012 *Phys. Rev. B* **85** 144425

[33] Bulla R, Costi T A and Vollhardt D 2001 *Phys. Rev. B* **64** 045103

[34] Liu T and Cao Z X, 2013 arXiv: 1312.4606 [quant-ph]

[35] Sassetti M and Weiss U 1990 *Phys. Rev. Lett.* **65** 2262

[36] Egger R, Grabert H and Weiss U 1997 *Phys. Rev. E* **55** R3809

[37] Volker K 1998 *Phys. Rev. B* **58** 1862

[38] Costi T A and Kieffer C 1996 *Phys. Rev. Lett.* **76** 1683

[39] Keil M and Schoeller H 2001 *Phys. Rev. B* **63** 180302

[40] Florens S, Venturelli D and Narayanan R 2010 *Lect. Notes Phys.* **802** 145

[41] Zhao C J, Lü Z G, and Zheng H 2011 *Phys. Rev. E* **80** 011114

[42] Gan C and Zheng H 2009 *Phys. Rev. E* **80** 041106

[43] Vojta M, Tong N H and Bulla R 2005 *Phys. Rev. Lett.* **94** 070604

[44] Vojta M, Tong N H and Bulla R 2009 *Phys. Rev. Lett.* **102** 249904(E)